Impacts of anthropogenic heat on summertime rainfall in Beijing

Article

Published Version

Impacts of Anthropogenic Heat on Summertime Rainfall in Beijing

WANSHU NIE

State Key Laboratory of Hydro-Science and Engineering, Department of Hydraulic Engineering, Tsinghua University, Beijing, China, and Department of Earth and Planetary Sciences, The Johns Hopkins University, Baltimore, Maryland

BENJAMIN F. ZAITCHIK

Department of Earth and Planetary Sciences, The Johns Hopkins University, Baltimore, Maryland

GUANGHENG NI AND TING SUN

State Key Laboratory of Hydro-Science and Engineering, Department of Hydraulic Engineering, Tsinghua University, Beijing, China

(Manuscript received 21 July 2016, in final form 5 December 2016)

ABSTRACT

Anthropogenic heat is an important component of the urban energy budgets that can affect land surface and atmospheric boundary layer processes. Representation of anthropogenic heat in numerical climate modeling systems is therefore important when simulating urban meteorology and climate and has the potential to improve weather forecasts, climate process studies, and energy demand analysis. Here, spatiotemporally dynamic anthropogenic heat data estimated by the Building Effects Parameterization and Building Energy Model (BEP-BEM) are incorporated into the Weather Research and Forecasting (WRF) Model system to investigate its impact on simulation of summertime rainfall in Beijing, China. Simulations of four local rainfall events with and without anthropogenic heat indicate that anthropogenic heat leads to increased rainfall over the urban area. For all four events, anthropogenic heat emission increases sensible heat flux, enhances mixing and turbulent energy transport, lifts PBL height, increases dry static energy, and destabilizes the atmosphere in urban areas through thermal perturbation and strong upward motion during the prestorm period, resulting in enhanced convergence during the major rainfall period. Intensified rainfall leads to greater atmospheric dry-down during the storm and a higher poststorm LCL.

1. Introduction

We live in a rapidly urbanizing world. This fact has motivated research in multiple fields concerned with environmental conditions in cities and the impact that cities have on the broader environment (Santamouris 2013; Wilby and Perry 2006). One area of interest is the impact that cities have on local and regional climate, including precipitation, because of the influence that urban land cover and urban activities have on land–atmosphere interactions and conditions in the planetary boundary layer (PBL; Mahmood et al. 2014). Researchers have investigated the spatiotemporal variability of surface–atmosphere exchanges within and between cities through field measurements (Grimmond and Oke 2002; Grimmond et al. 2004; Masson et al. 2002) and numerical simulations (Arnfield 2003; Arnfield and Grimmond 1998; Chen et al. 2014; Miao et al. 2009). Besides the urban morphology, cities could also influence the regional turbulent and chemical transport through the waste heat and pollutant emissions. The impact of heat fluxes and pollutants on urban meteorology and air quality have been studied worldwide, including in China (Feng et al. 2012; Yu et al. 2014), Japan (Narumi et al. 2009), the United States (Fan and Sailor 2005; Gutiérrez et al. 2013), Australia (Simmonds and Keay 1997), and European countries (Flanner 2009; Rosenfeld 2000). These interactions have brought widely concerned climate issues such as the urban heat island (UHI) effect, the modification of rainfall frequency and pathways, and the climate-related threats to human health.

Corresponding author e-mail: Ting Sun, sunting@tsinghua.edu.cn

DOI: 10.1175/JHM-D-16-0173.1

One key focus for these studies is the surface energy balance of urban surfaces, which is usually formulated as follows:

$$R_n + Q_F = H + \mathrm{LE} + G + Q_A, \quad (1)$$

where R_n is all-wavelength net surface radiation, H is sensible heat flux, LE is latent heat flux, G is ground heat flux, and Q_A is net advection, which is generally assumed to be negligible relative to the other terms (Sailor 2011). Variable Q_F is anthropogenic heat (AH), a term that is often neglected in natural or sparsely populated settings but that can be a significant term in the surface energy balance in urban environments (Sailor 2011; Taha 1997). Indeed, the magnitude of Q_F has been found to be comparable to R_n under some conditions (Hamilton et al. 2009; Nie et al. 2014).

A number of studies have investigated the implications of AH on the thermal environment of cities. In a study of Tokyo, Ichinose et al. (1999) found that Q_F in central Tokyo could be as large as 1590 W m^{-2} in winter and nearly 400 W m^{-2} in summer, leading to an increase in nocturnal air temperature of about 2°–3°C in winter and 1.5°C in summer. Similarly, Bohnenstengel et al. (2014) found that AH can result in increases in the UHI intensity of London by 1° and 1.5°C in May and December, respectively. In a study of Hangzhou, Chen et al. (2016) found Q_F contributes to 65% and 17% of the UHI in winter and summer, respectively, using the Weather Research and Forecasting (WRF) Model (Skamarock et al. 2005) with a spatially heterogeneous anthropogenic heat dataset. Modeling studies that have accounted for Q_F have found that including AH improves the simulation of urban temperatures when compared to available observations (Benson-Lira et al. 2016; Best and Grimmond 2016; Chen et al. 2016; Yu et al. 2014).

A parallel line of research has addressed the influence that cities might have on local and regional precipitation. There is evidence that urbanization is associated with increased frequency of heavy rainfall in cities, as diagnosed in observational studies from the United States (Ashley et al. 2012; Changnon and Westcott 2002; Haberlie et al. 2015) and India (Kishtawal et al. 2010), among others. A number of mechanisms have been proposed for this phenomenon, one of which is anthropogenic land-cover change. Pielke et al. (2007, 2011) present the most recent review and evidence of regional land use, including the impact of urban land-cover change on precipitation. Urban parameterizations in weather-forecasting models have shown that urban surface heterogeneity has the potential to influence surface temperature, vertical wind, and storm initiation (Lei et al. 2008; Nobis 2007). The Metropolitan Meteorological Experiment (METROMEX) examined mesoscale effects of large cities on convective rainfall and concluded that enhancement of rainfall downwind of the city center could be attributed to both the UHI, which leads to reduced stability in the planetary boundary layer, and increased surface roughness (Cadet 1983; Thielen et al. 2000). The presence of precipitation anomalies downwind of an urban center to the urban effect was also found in long-term studies of Oklahoma City (Hand and Shepherd 2009; Niyogi et al. 2006) and Indianapolis (Niyogi et al. 2011). The UHI was also identified as an important factor for enhanced convergence during precipitation events over cities in studies of Atlanta (Bornstein and Lin 2000), New York City (Bornstein and LeRoy 1990), Houston (Shepherd and Burian 2003), and Nashville (Shepherd et al. 2002).

At the same time, other studies have found that cities lead to reductions in precipitation. For instance, the expansion of impervious urban surfaces could diminish evapotranspiration and thus reduce atmospheric water vapor, resulting in less convective available potential energy (CAPE) and decreased summer rainfall (Zhang et al. 2009). It is also reported that cities could reduce rainfall through an urban building barrier effect, in which storms bifurcate around a city, resulting in less precipitation over the urban core (Guo et al. 2006). Urban aerosols could also influence the precipitation processes, though the mechanism and direction of that influence is not yet known (Ryu et al. 2013; Yu et al. 2014). Aerosols could promote rainfall because of increased availability of cloud condensation nuclei (CCN), favoring deeper cloud convection (Andreae et al. 2004; Diem and Brown 2003; Johnson 1982), but they could also suppress rainfall by reducing incoming solar radiation, thus decreasing available energy for evaporating water and for energizing convective clouds (Ramanathan et al. 2001; Rosenfeld et al. 2008).

Few studies have directly addressed the role that AH, via its influence on the UHI, might play in urban impacts on precipitation. Among them, two recent studies of Chinese cities produce contradictory results in the same area: Chen et al. (2016) found that the combined impact of urbanization and AH increased precipitation in Hangzhou city by 1.2% in winter and 14.4% in summer because of the enhancement of low-level convergence, while Feng et al. (2012) reported a noteworthy decrease in precipitation in the Yangtze River delta region (including Hangzhou city). It is also interesting to note that the combined factors of urbanization and AH may result in opposite impact on precipitation in different urban areas. For instance, though Feng et al. (2012) found that

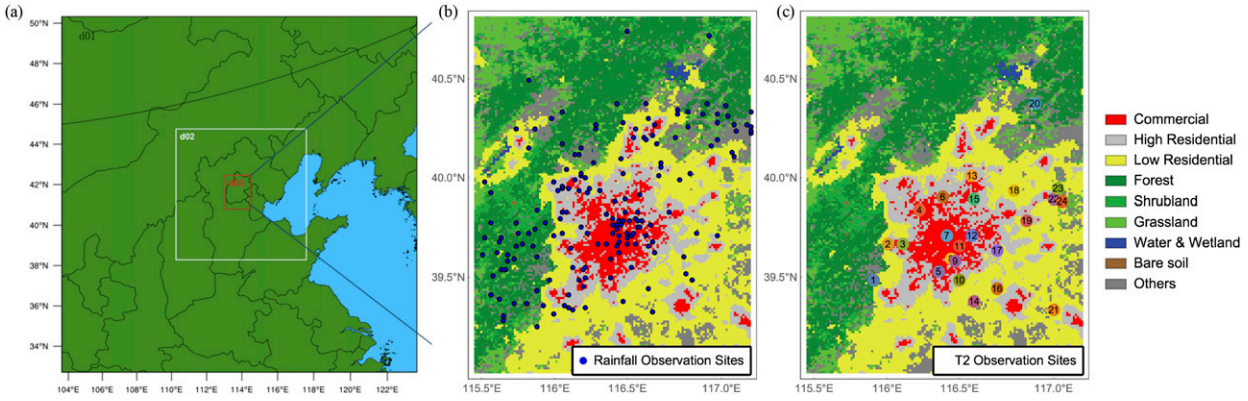

FIG. 1. WRF simulation configuration of (a) one-way nested domains and (b) the land-cover map for the innermost domain (D03) with rainfall observational sites and (c) with 2-m air temperature observational sites.

AH reduced precipitation in the Yangtze River delta region, they also found that combined effects of urbanization and AH increase summer precipitation by 26.9% in the Beijing–Tianjin–Hebei region. They do not identify any clear mechanism for the inconsistent effect on urban precipitation because of the complexity of the system and the relatively coarse resolution of analysis. One possible reason for this disagreement may be the simplified representation of AH by the urban canopy model (UCM) used in these studies: the normalized AH diurnal profile is fixed for all three urban categories and cannot respond to atmospheric conditions; in other words, the AH diurnal cycle will always peak at the same time no matter if it rains heavily or it is bright and sunny. In addition, recent work has shown that it is important to represent AH in a manner appropriate to the scale of analysis (Sailor et al. 2015), which has not been considered in previous modeling studies. This points to the need for high-resolution modeling studies that include dynamic and spatial differentiable representation of AH pattern and that can be applied in a range of urban environments.

Here, to better understand the mechanism of AH impact on urban rainfall, we apply WRF to simulate summertime rainfall events in Beijing. Anthropogenic heat is simulated using the Building Effects Parameterization and Building Energy Model (BEP-BEM), which includes multilayer building–atmosphere interactions and can simulate spatial and temporal variability in AH as a function of meteorological conditions as well as fixed diurnal and land-use factors (Salamanca et al. 2010). This modeling system allows us to study the sensitivity of simulated precipitation to AH, to evaluate the impact that AH has on model performance relative to available observations, and to investigate mechanisms through which AH influences the convective environment.

2. Data and methodology

a. Description of the study area and simulation setup

The WRF Model, version 3.6.1, was applied to investigate the impact of anthropogenic heat on summertime precipitation in Beijing. WRF simulations in this study are conducted using three nested domains with horizontal grid increments of 9, 3, and 1 km, respectively (Fig. 1a). All the domains are centered at the Meridian Gate, Beijing (39.92°N, 116.39°E). The largest domain (D01) covers most of the northern China plain, the second domain (D02) includes Hebei Province and part of Shanxi and Shandong Provinces, and the innermost domain (D03) covers all of the Beijing metropolitan area and neighboring towns to its south. The model consists of 27 full sigma levels extending from the surface to 50 hPa.

WRF physics options in this study were informed by many previous applications of WRF to warm season mesoscale convection (Evans et al. 2012; Jankov et al. 2005; Yang et al. 2014). In particular, cloud microphysics and PBL parameterizations have been shown to have significant impacts on the simulation of precipitation under these conditions. Based on prior experience with WRF simulations of the Beijing area (Sun et al. 2016; Yu and Liu 2015), we selected an optimal set of WRF physics options (Table 1). Additional tests were performed to compare the microphysics parameterization and cumulus scheme settings, as these options are known to have a strong influence on the simulation of rainfall in Beijing (Yang et al. 2014), and these tests confirmed that the combination of the WRF single-moment 3-class (WSM3) microphysical scheme (Hong et al. 2004) and the cumulus-off option, as listed in Table 1, outperformed other options in WRF.

In addition, urban surface processes were included using a single-layer UCM in D01 and D02 and the

TABLE 1. Physics options used in WRF simulations.

Physical schemes	Option	Option index
Microphysics (mp_physics)	WSM3	3
Longwave radiation (ra_lw_physics)	RRTM	1
Shortwave radiation (ra_sw_physics)	MM5	1
Land surface (sf_surface_physics)	Noah	2
Urban surface (sf_urban_physics)	UCM (D01), UCM (D02), and BEP-BEM (D03)	1, 1, 3
PBL (bl_pbl_physics)	MYJ	2
Cumulus (cu_physics)	Off	0

BEP-BEM in D03. Both UCM and BEP-BEM considered the urban surface heterogeneity with three land-cover categories: low-density residential area, high-density residential area, and commercial area, with impervious fractions of 50%, 90%, and 95%, respectively. Although both UCM and BEP-BEM could estimate AH release in urban areas, compared to the prescribed/static AH profiles in single-layer UCM, BEP-BEM can dynamically predict AH release based on the outdoor and indoor environment in conjunction with WRF and thus allows direct interactions between the urban surface and PBL. For example, BEP-BEM accounts for variability of building heights within and between urban land-use types. This means that the parameterization of a single urban grid cell accounts for variable building heights, and the distribution of building heights also differs for the three different urban land-use types. This variation in buildings allows for the spatial distribution of anthropogenic heat emission in both horizontal and vertical directions.

As noted earlier, AH in UCM is assumed to follow a fixed diurnal pattern, with a peak value of $20\,W\,m^{-2}$ for low-intensity residential (LIR) area, $50\,W\,m^{-2}$ for high-intensity residential (HIR) area, and $90\,W\,m^{-2}$ for commercial area (CIT). This assumption may bring unreasonable results, especially when one concentrates on meteorological impacts of urban areas in hot summer and cold winter days. Anthropogenic heat emission from buildings is dominated by heating, ventilation, and air conditioning (HVAC) systems (Sailor 2009, 2011), and the energy consumption of these systems is greatest on hot days [air conditioning (AC)] and cold days (heating). In BEP-BEM, however, AH is coupled with atmospheric processes and is calculated based on indoor temperature and air humidity settings, HVAC time schedules, and indoor population density (Salamanca et al. 2010). This means that AH due to cooling and heating systems, and associated equipment energy consumption in buildings, is predicted by the model and varies with time. We use an indoor target temperature of 298 K, which is consistent with standard temperature control for public buildings in Beijing. It is also the default setting in BEM. Because AH emission of AC systems dominates meteorology-based variability in electric consumption in a semiarid metropolitan area (Salamanca et al. 2013), it is critical to consider the building energy consumption and atmosphere interactions for hot summer events.

It should be noted that BEP-BEM is designed specifically to simulate building energy and thus cannot provide AH emission from the transportation sector. However, specifically for Beijing, we did quantify the AH values due to transportation at different scales. First, in Nie et al. (2014), we estimated the AH from transportation of the Tsinghua campus under different scenarios, which indicates a daily maximum Q_F of $\sim 45\,W\,m^{-2}$ under the moderate scenario (i.e., normal business) at the street scale (~20 m). Second, in Nie (2015), we used the traffic information extracted from an online map service to estimate the spatiotemporal characteristics of AH from transportation of the Beijing core urban area, which suggests a daily mean Q_F of $\sim 4\,W\,m^{-2}$ at the district scale (~1 km). Because of the relatively minor contribution of transportation to the total AH in Beijing, we thus deem that in this study AH from buildings is a reasonable approximation of total AH.

We isolate the influence of AH on WRF simulations of summertime precipitation events by performing control simulations without anthropogenic heat (AH_{OFF}) and identical simulations with anthropogenic heat included (AH_{ON}). The AH_{ON} simulations use BEM defaults to estimate heat emission as a function of meteorology.

b. Land-cover update

The representation of urban surfaces is one key element in mesoscale NWP models because of its significant impact on the urban–atmosphere interactions (Grimmond et al. 2010) and related processes [e.g., precipitation (Shepherd 2005) and air pollution transport (Rosenfeld et al. 2008)]; another key factor for urban simulations is the appropriate land-use dataset. Given the land-use data embedded in WRF (USGS 24 of 1992/93 and MODIS of 2004) are out of date for present scenarios, a land-use map of Beijing was

generated to more accurately describe the urban surface as well as the spatial distribution of AH sources.

The Operational Linescan System (OLS) sensor under the Defense Meteorological Satellite Program (DMSP) was originally designed to observe nighttime cloud cover for meteorological forecasting. Since the sensor is also sensitive to low-intensity visible and near-infrared light sources, a ''city light'' algorithm was developed for DMSP-OLS data (Elvidge et al. 1997) and has been applied to the urban land-use categorization, population and economic growth estimation, and other urban studies [refer to Huang et al. (2014) for a review]. In this study, an annual cloud-free stable light composite product with digital numbers (DNs) for 2013 (data available at ngdc.noaa.gov/eog/) was chosen for categorizing the up-to-date land use in Beijing. The product has been quality controlled, with the background noise, fires, and ephemeral lights removed (Baugh et al. 2010).

Although the nighttime dataset works well in distinguishing urban boundaries, additional information of pervious surface fraction for each urban grid cell is needed to further categorize subgrid land-use types. To satisfy this need, the *Terra* MODIS normalized difference vegetation index (NDVI) dataset MOD13A3 (temporal and spatial resolutions of month and 1 km, respectively) of 2013 was used to estimate pervious surface fractions. The combined DMSP-OLS and MOD13A3 data were then used to derive detailed urban land-cover information of Beijing. Because of the spatial resolution inconsistency between DMSP-OLS (30 arc s) and MOD13A3 (1 km), DMSP-OLS was unscaled to 1 km as MOD13A3 using a bilinear interpolation algorithm. Both satellite data are then reprojected to a Lambert conic conformal projection to match the coordinate system of the WRF domains.

Following Lu et al. (2008) and Chen et al. (2014), human settlement index (HSI) was used to classify urban land cover based on a combination of DMSP-OLS satellite nighttime light data and MODIS NDVI, whose key steps are recapitulated as follows:

1) The normalized value of nighttime light data $\mathrm{OLS_{nor}}$ is defined as

$$\mathrm{OLS_{nor}} = \frac{\mathrm{OLS} - 20}{\mathrm{OLS_{max}} - 20}, \tag{2}$$

in which OLS represents the original DN value of the product, ranging from 1 to 63. A threshold of 20 was selected instead of 1 in order to minimize the effect of blooming.

2) To account for cloud contamination and seasonal vegetation, the maximum value of NDVI for each grid, namely, $\mathrm{NDVI_{max}}$, for the whole year is chosen as

$$\mathrm{NDVI_{max}} = \max(\mathrm{NDVI_1}, \mathrm{NDVI_2}, \ldots, \mathrm{NDVI_{12}}), \tag{3}$$

in which the subscripts of NDVI denote the calendar months of a year.

3) The HSI for each grid cell is calculated as

$$\mathrm{HSI} = \frac{(1 - \mathrm{NDVI_{max}}) + \mathrm{OLS_{nor}}}{(1 - \mathrm{OLS_{nor}}) + \mathrm{NDVI_{max}} + \mathrm{OLS_{nor}} \times \mathrm{NDVI_{max}}}. \tag{4}$$

As can be seen, for example, a large $\mathrm{OLS_{nor}}$ in together with a small $\mathrm{NDVI_{max}}$ would result in large HSI, indicating a densely built-up area with a relatively small fraction of vegetation.

4) HSI thresholds are set based on sample locations across Beijing: (i) grids with HSI greater than 95% represent CIT, (ii) grids with HSI between 85% and 95% represent HIR, and (iii) grids with HSI between 55% and 85% represent LIR.

5) This classification was superimposed on the MODIS 20-category land-use dataset to represent the up-to-date surface characteristics of Beijing, as shown in Fig. 1b.

By applying HSI as an indicator to classify the urban land-use types instead of simply using the nighttime light data, urban land classes could be represented more precisely. The combination of NDVI and the nighttime light data is particularly valuable in rapidly growing developing cities, as the nighttime lights alone sometimes miss newly urbanized areas that have relatively low levels of nighttime lighting.

For grid cells classified as LIR, HIR, or CIT, the BEP-BEM module is called in WRF to calculate anthropogenic heat from five basic sources: sensible heat from AC systems, latent heat from AC systems, sensible heat from ventilation, latent heat from ventilation, and energy consumption from electrical equipment. Note that the three types of urban grid cells are not fully covered with built surface. Therefore, the spatial distribution of anthropogenic heat not only depends on the climate forcing, but also the impervious fraction of each type of grid cell. For the sensible heat and latent heat from HVAC system, BEP-BEM calculates the flux based on various parameters, including heat source from the AC system, air density, specific heat at constant pressure, a link parameter between the mesoscale and urban scale, and other factors. Energy consumption from electrical equipment is set as a fixed profile in which the peak value is a function of urban land-cover type, that is, electricity consumption is not sensitive to meteorology, but it does depend on the working schedule of the buildings. Figure 2 provides a simplified summary of the estimation of anthropogenic heat in BEM and its communication to WRF via surface fluxes.

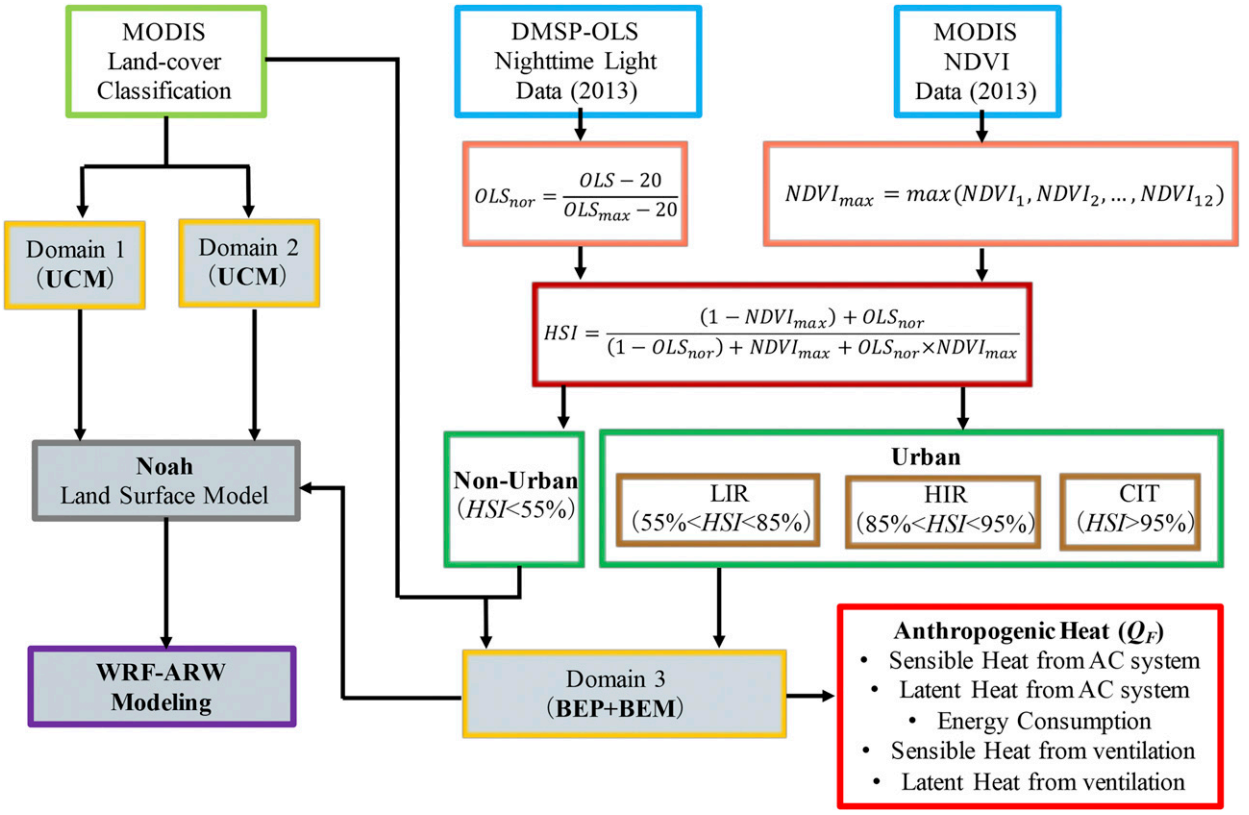

FIG. 2. Flowchart for updating the land-cover map based on DMSP-OLS nighttime light data and MODIS NDVI data and estimating AH in BEP-BEM.

c. *Selected events*

In this study, rainfall events are selected that satisfy the following patterns: 1) maximum temperature during each rainfall event exceeds 28°C as a representative of warm convection events in order to capture the characteristics of summertime rainfall during high AH emission days and 2) the major convection period appears in the warm afternoon during which the atmosphere is unstable because of daytime heating and updraft motion. To identify a rainfall event, three periods are distinguished: a 6-h prestorm period, a major convective rainfall period, and a 6-h dry-down period. Thresholds of 0.5 and 0.1 mm h^{-1} are set as the initial and terminal rainfall intensities, respectively, to identify the major convective rainfall period. Based on the above criteria, four summertime events are identified in 2014 and 2015: 1) 0700 local time (LT) 1 July to 0400 LT 2 July 2014, 2) 1000 LT 2 July to 0100 LT 3 July 2014, 3) 1000 LT 27 July to 1300 LT 28 July 2015, and 4) 1300 LT 29 July to 0700 LT 30 July 2015. Figure 3 shows a snapshot of the synoptic weather conditions (geopotential height at 500 hPa) in the prestorm period for each event. In all four events there is a low pressure center to the north of Beijing. For events 1 and 4, the trough is significant and crosses domain 3 over the course of the event (not shown), indicating a significantly unstable atmospheric condition and synoptically controlled rainfall processes affecting central Beijing. In contrast, for events 2 and 3, there is only a weak low pressure system, and the trough stays to the north of the city throughout the rainfall event, indicating that the synoptic patterns of these two events are almost stationary. For these events synoptic forcing of rainfall is less extreme, so local convection may play a greater role. This study focuses on understanding the impact of anthropogenic heat on the magnitude and spatial distribution of rainfall across all four events, but further analysis of a larger population of synoptic weather patterns could provide further insight on differences in the influence that AH has on different types of rainfall processes.

The in situ observational precipitation data for D03 are provided by the Ministry of Water Resources, China. It is worth noting that some of the observation sites have been updated and relocated during the study time period; therefore, the available observation sites for each event are different. For both events 1 and 2, 38 urban observation stations are applied, but 153 sites are available to capture the meteorological conditions of

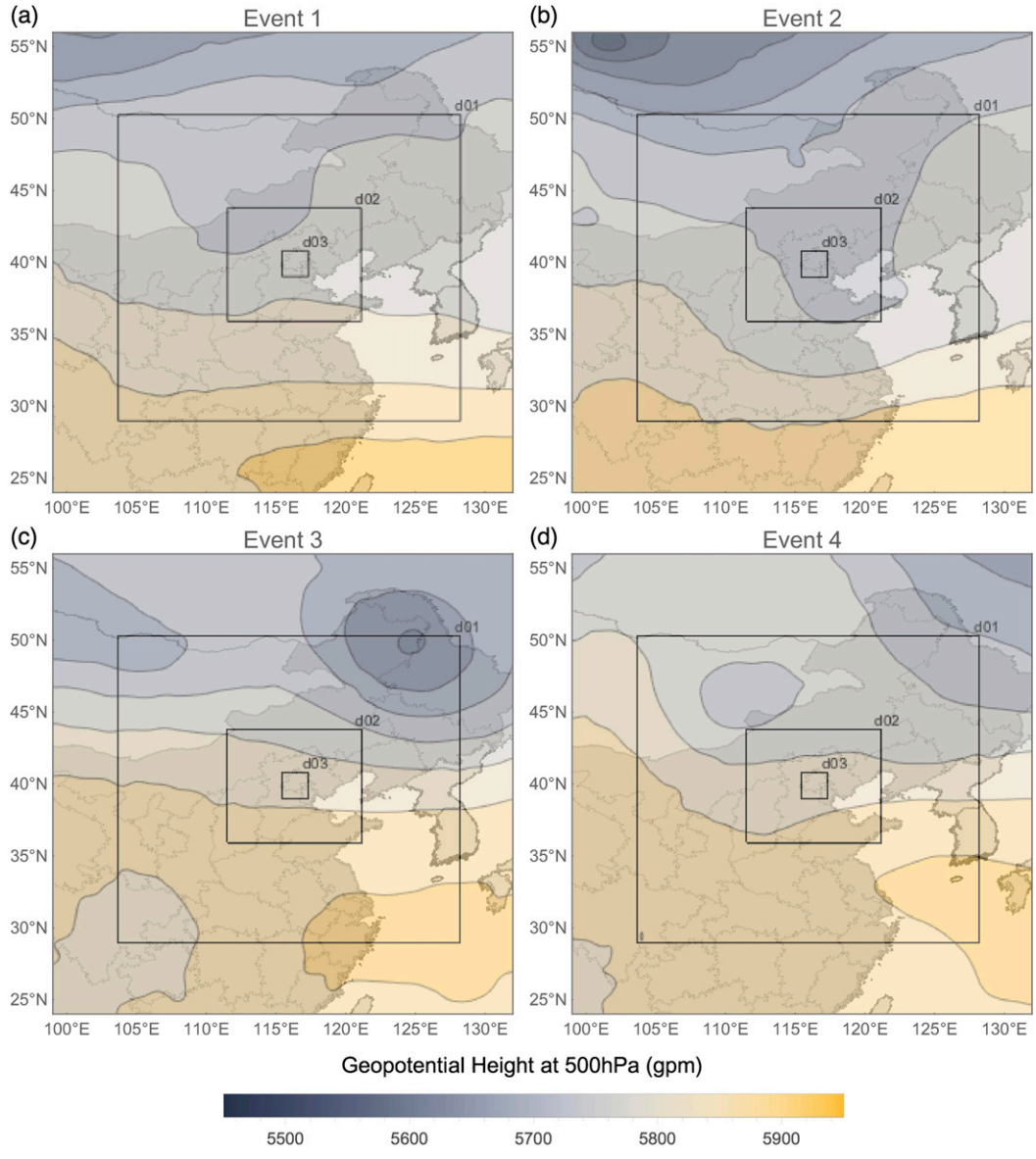

FIG. 3. The synoptic weather pattern of geopotential height at 500 hPa for (a) 0800 LT 1 Jul 2014, (b) 1400 LT 2 Jul 2014, (c) 1400 LT 27 Jul 2015, and (d) 1400 LT 29 Jul 2015.

event 3, and 86 sites are available for event 4. The locations of all observation sites are shown in Fig. 1b.

The in situ observational 2-m air temperature data for D03 are provided by the China Meteorological Administration (CMA); 24 sites located in the urban area (Fig. 1c) with full records of the four events are selected for model evaluation.

3. Results and discussion

a. Model evaluation

Simulations were evaluated against CMA precipitation observations for all four events (Table 2). WRF–UCM–BEM simulations without AH underestimate cumulative precipitation for all events except event 4. Including AH increases total precipitation for all four simulated rain events. This results in a decrease in bias for the two large rainfall events (events 1 and 3) but a small increase in bias for the light rainfall events (events 2 and 4). The total impact of AH for large rainfall measurements is to reduce WRF bias in the simulation of urban precipitation during these warm, high AH days, suggesting that including AH in simulations of urban precipitation could contribute to improved model performance under these conditions. Of course, it is also possible that other model factors are

TABLE 2. Comparison of the observed and simulated cumulative rainfall (mm) for each event [observation (obs), simulation in AH_{ON} (AH_{ON}), simulation in AH_{OFF} (AH_{OFF}), and the ratio of RMSE and standard deviation of the observations (RMSE/σ_{obs})].

	Mean value			Bias		Std dev			RMSE		RMSE/σ_{obs}	
	μ_{obs}	$\mu_{AH_{ON}}$	$\mu_{AH_{OFF}}$	$\Delta_{AH_{ON}}$	$\Delta_{AH_{OFF}}$	σ_{obs}	$\sigma_{AH_{ON}}$	$\sigma_{AH_{OFF}}$	$E_{AH_{ON}}$	$E_{AH_{OFF}}$	$E_{AH_{ON}}/\sigma_{obs}$	$E_{AH_{OFF}}/\sigma_{obs}$
Event 1	20.2	18.0	11.7	−2.2	−8.5	9.6	6.3	5.3	11.4	15.1	1.2	1.6
Event 2	1.6	5.6	0.2	4.0	−1.4	1.2	4.9	0.3	6.0	1.9	5.0	1.6
Event 3	12.8	13.8	8.2	0.9	−4.7	18.1	12.0	9.0	20.2	19.3	1.1	1.1
Event 4	7.8	12.7	9.6	4.9	1.9	10.9	12.2	12.8	16.7	16.1	1.5	1.5

responsible for rainfall underestimates in AH_{OFF} and that including AH simply corrects for these unrelated model biases. Indeed, including AH led to an overestimate of rainfall during the smaller rain events (events 2 and 4), making it difficult to make conclusive statements about the contribution of AH to overall model skill. As pointed out by Pielke and Mahrer (1978), the ratio of root-mean-square error (RMSE) to the standard deviation of observations σ_{obs} for both AH_{ON} and AH_{OFF} exceeds 1 for all the events, indicating that our convection-permitting WRF Model has limited skill in localizing convective rainfall. This may be due to defective ensemble physical schemes or to unrealistic simplification of the model calculation.

Surface air temperatures (at 2 m above ground level, hereinafter T_2) were evaluated against observations from 24 sites for all four events. Simulated patterns of T_2 variability in both AH_{ON} and AH_{OFF} show overall agreement with the observations, with correlation coefficient at most sites >0.8 for all events except event 1 (Fig. 4). As can be seen from the normalized standard deviation (i.e., simulated standard deviation normalized by that of observation), WRF performance for the absolute values of distributed T_2 was strong for event 3 but lower for other events; the timing was off for event 1, while the magnitude of peak T_2 was incorrect for events 2 and 4.

A full evaluation of all the factors influencing WRF performance in the Beijing environment is beyond the scope of the study. Here we simply conclude that, for the four studied events, including AH does not degrade WRF performance. In the following section, we explore the general influence that AH has on the simulated urban energy balance, PBL properties, atmospheric stability before and during the rainfall period, and resulting impacts on spatiotemporal rainfall distribution.

b. *AH influence on urban energy balance*

Figure 5 (left) shows the spatially averaged diurnal cycle in AH_{ON} for each urban land-cover class and for the all-urban average of all four events. The maps

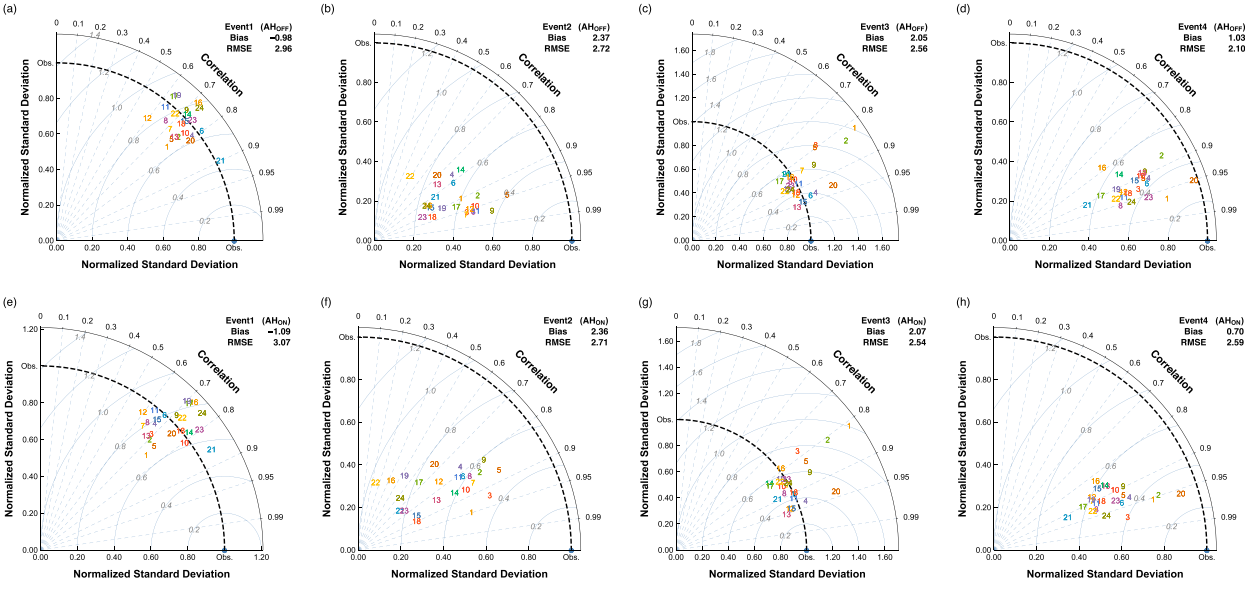

FIG. 4. Evaluation of WRF performance for (a) event 1, (b) event 2, (c) event 3, and (d) event 4 in AH_{OFF} and (e) event 1, (f) event 2, (g) event 3, and (h) event 4 in AH_{ON}. Statistics include correlation, normalized standard deviation, and normalized RMSE shown in the Taylor diagram plus average bias and RMSE.

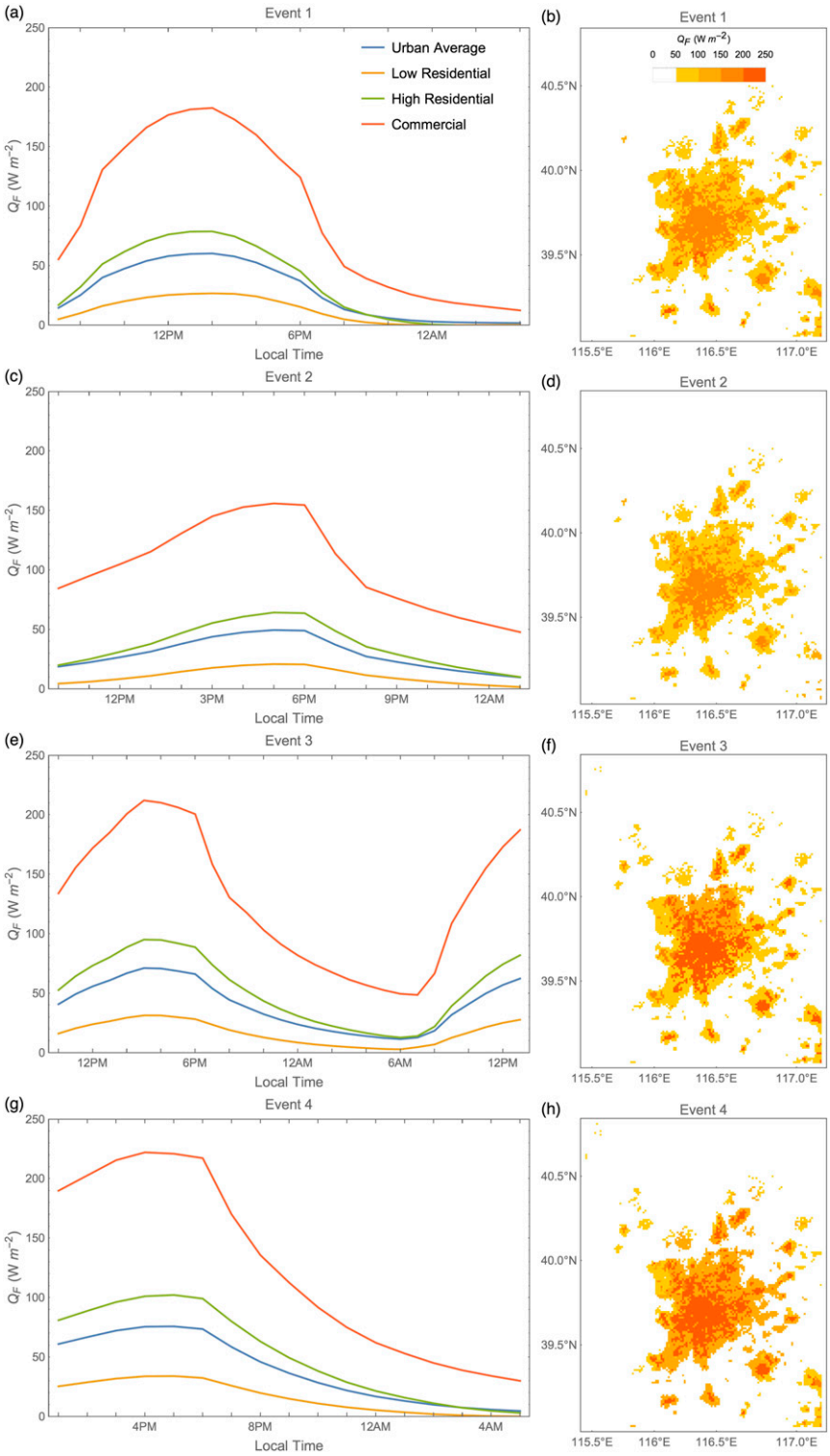

FIG. 5. Spatially averaged diurnal cycle in AH_{ON} for each urban land-cover class and for the (left) all-urban average and (right) peak hour AH map for each event.

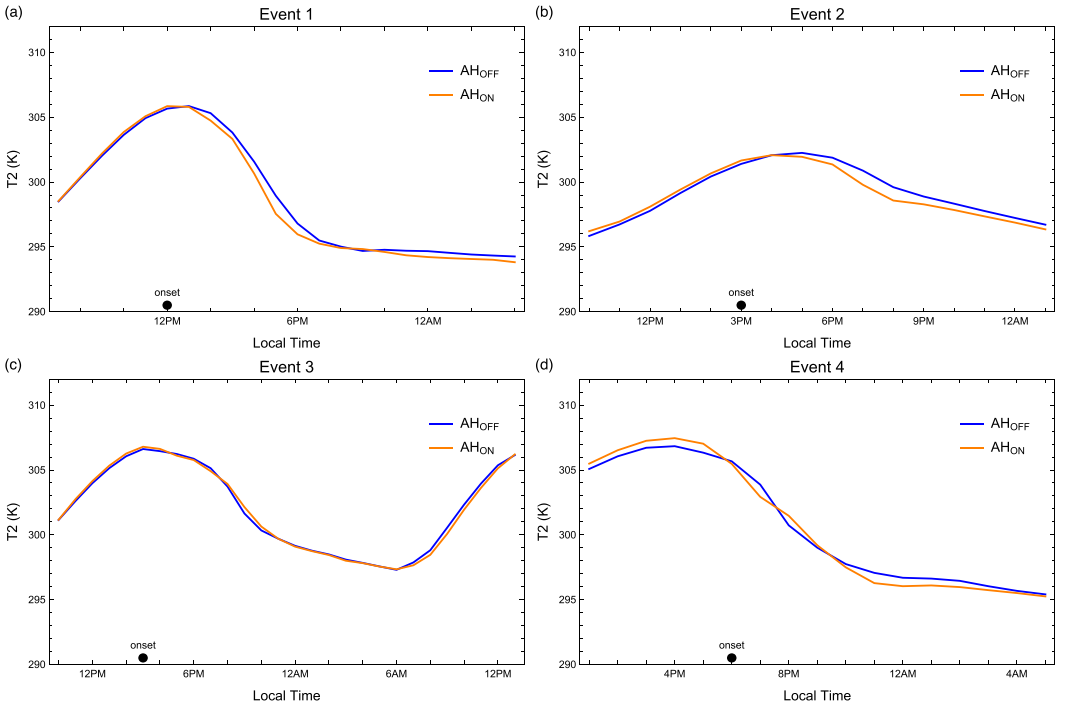

FIG. 6. Temporal profile of urban-averaged 2-m air temperature in AH_{ON} and AH_{OFF} for each event.

(Fig. 5, right) show the peak hour spatial pattern of AH of all events. Sensible heat emissions from air conditioning dominate the AH mix (nearly 80% of total), and as a result total AH sensible heat flux far exceeds AH latent heat flux. As shown in Fig. 5, the area of higher building density has higher AH values. For example, for the warm convection event 3, though the urban-averaged AH is only 40.6 $W m^{-2}$, that of the commercial area reaches 128.4 $W m^{-2}$, indicating a large spatial difference as shown in Fig. 5f. The peak of AH always appears in the late afternoon or early evenings instead of noon, reflecting the timing of maximum air-conditioning loads. To first order, simulated AH follows T_2, reacting to the need for temperature control in buildings. There is a second-order feedback, however, as AH does have a systematic impact on T_2 averaged across the urban area across the rainfall event (Fig. 6). Slightly greater T_2 is found in AH_{ON} for all the events before the onset of rainfall, reflecting the contribution of AH to air temperature. However, AH_{ON} exhibits stronger surface cool down after the onset of convection. This may be due to the fact that convection is stronger in AH_{ON}, with rising motion and import of moist, cooler air. The faster cool-down process, in turn, reduces the emission of AH by reducing the difference of the outdoor and indoor air temperature, resulting in a positive feedback on cooling.

The diurnal AH cycle is worth noting because it implies that AH impacts are most likely for afternoon convection. In addition, the spatiotemporal characteristics of AH estimated by the BEP-BEM vary in each event as a function of dynamic atmospheric conditions, providing a more dynamic representation of AH distribution compared to the fixed AH profile setting in UCM. However, it should be noted that a precise representation of AH highly depends on the skill of WRF to capture the timing and magnitude of the air temperature within the urban canyon. Our results show that WRF simulations were able to capture the timing of surface air temperature for all the events except event 1, but that there were errors in the simulation of the magnitude of air temperature, except for event 3.

In WRF simulations for all the selected events, including AH leads to an increase in daytime sensible heat and ground heat flux in urban areas but has little impact on latent heat flux [Fig. 7; see also Eq. (1)], confirming that AH influence on the atmosphere in these simulations is primarily via sensible heat. To further explore AH impact on sensible heat, the hourly averaged spatial difference of sensible heat (AH_{ON} minus AH_{OFF}) for each event is shown in Fig. 8. In general, the peak area of sensible heat increase is located in the commercial area, which is consistent with the spatial pattern of AH.

It should be noted that although AH makes almost no contribution to latent heat (less than 5%) in this study, this result depends on the energy consumption method. For cooling via AC system, latent AH is negligible, but

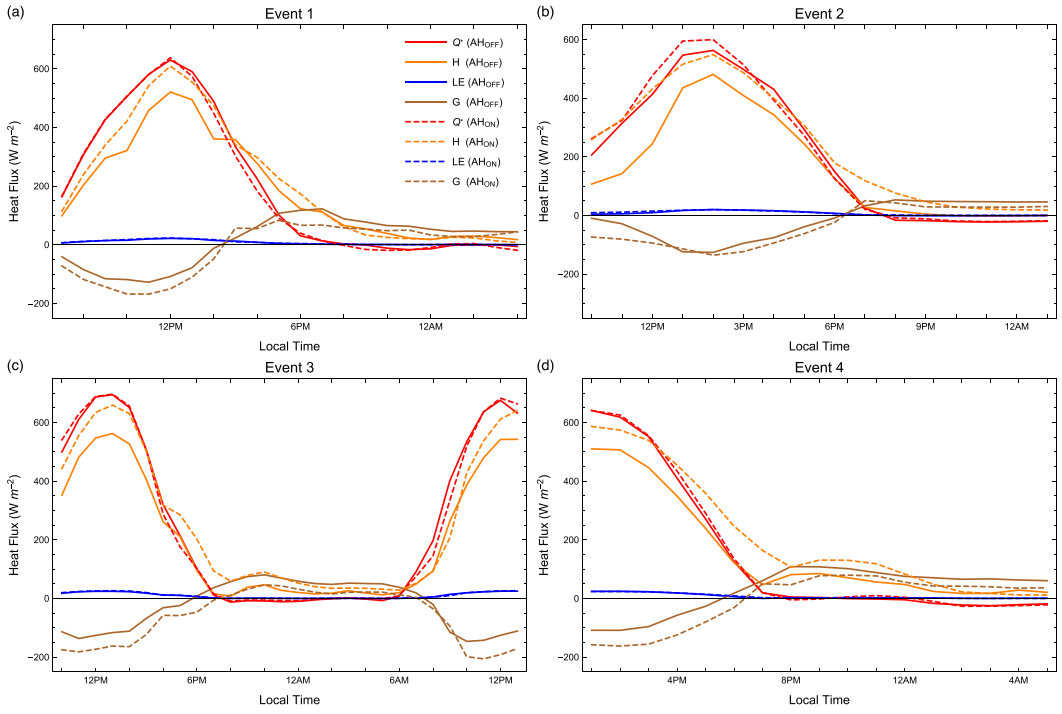

FIG. 7. Temporal profile of urban-averaged sensible heat, latent heat, and ground heat fluxes for each event in AH_{ON} and AH_{OFF}. Urban and commercial AH are also denoted in the figure.

anthropogenic activities such as the use of evaporative cooling equipment or chemical reactions involving water release can produce substantial latent heat flux to the atmosphere.

c. *AH influence on atmospheric boundary layer*

To investigate the anthropogenic heat influence on the atmospheric boundary layer, we examine PBL height, lifting condensation level (LCL), and moist static energy (MSE) density within PBL in AH_{ON} versus AH_{OFF} simulations for each event. In our study, the MYJ PBL scheme is used, which determines the PBL height from prognostically calculated turbulent kinetic energy (TKE). The top of the PBL is defined to be the height where the TKE decreases to a prescribed low value (Janjić 1994). Urban-averaged PBL heights in the prestorm period in AH_{ON} are systematically greater than AH_{OFF} for all the events (Fig. 9). For example, the average PBL height growth in the urban area is nearly 100 m higher in AH_{ON} in the prestorm period for event 2, which could substantially change mixing conditions, considering that the average PBL height is only 885.4 m. The effect is even greater in the commercial area, where AH is greatest (Table 3).

Unlike the PBL height, the LCL difference between the two simulations, especially for events 1 and 4, tends to emerge in the dry-down period, after the rainfall peak. This pattern is indicative of more intense convection and greater rainfall rates in AH_{ON} relative to AH_{OFF}, leading to greater atmospheric dry-down and a higher postevent LCL. Interestingly, impacts of AH on prestorm MSE density in the lower atmosphere are negligible (Table 3), as the contribution of AH to thermal energy (c_pT, with c_p the heat capacity of air and T the air temperature) is approximately counterbalanced by the deepening of the PBL and associated entrainment of lower energy air from the free troposphere. Since AH is almost entirely sensible in these simulations, changes in latent energy (Lq) are small; the slightly smaller latent energy in AH_{ON} for most events reflects the fact that the PBL is drier because of the deepening of the PBL.

d. *AH influence on atmospheric stability*

To investigate the anthropogenic heat influence on atmospheric stability in the urban area, the vertical gradient of potential temperature θ, equivalent potential temperature θ_e, and pressure velocity ω in the prestorm period are evaluated for all events (Table 3). In all cases, the vertical gradient of θ in the lower atmosphere ($\Delta\theta = \theta_{2000\text{m}} - \theta_{500\text{m}}$) is positive, while the vertical gradient of θ_e is negative, indicating conditionally stable boundary layer conditions during the prestorm period. However, AH warms the near-surface environment, leading to a decrease (increase) in the magnitude of $\Delta\theta$ ($\Delta\theta_e$) for all four

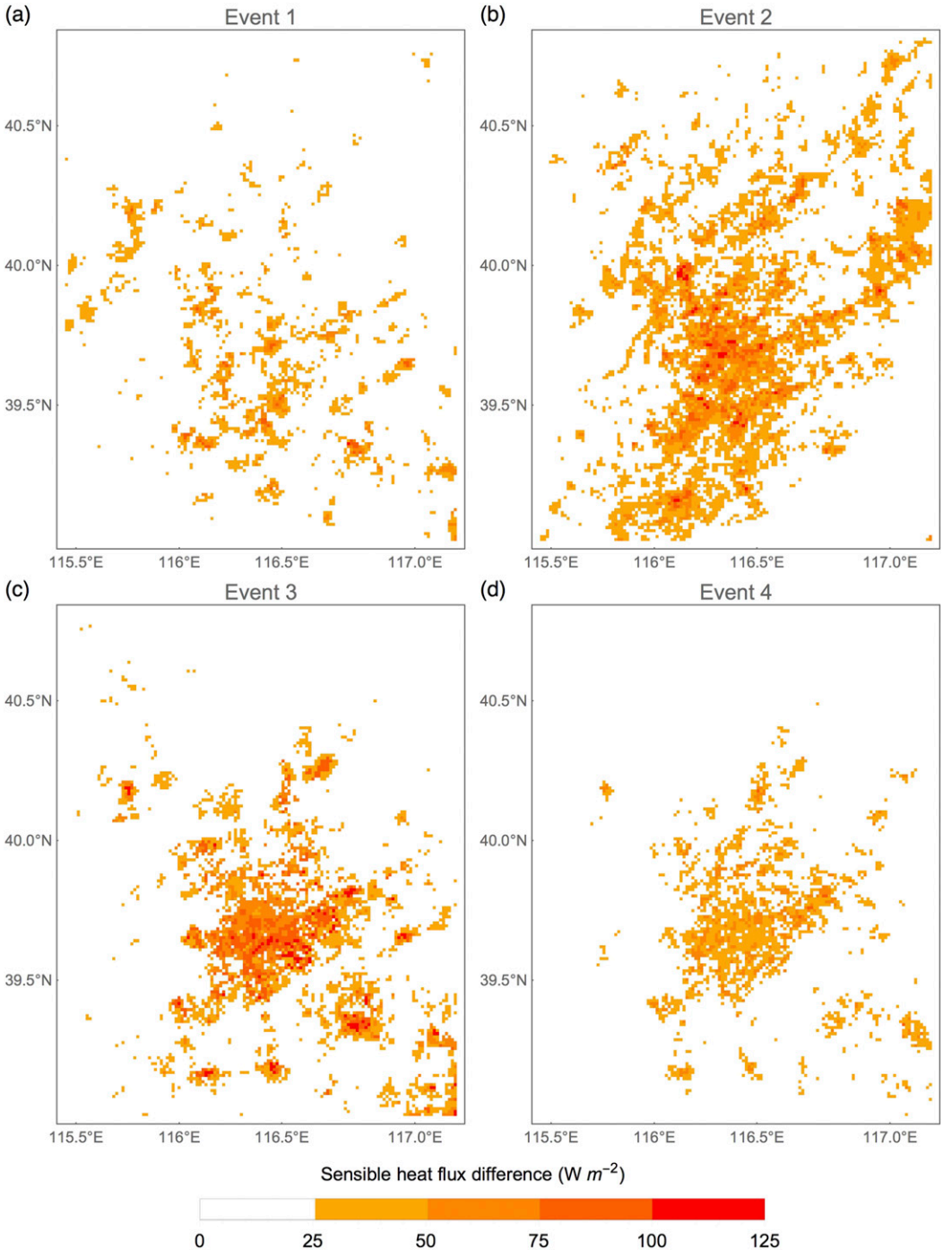

FIG. 8. Hourly average spatial distribution of the difference of sensible heat (AH_{ON} minus AH_{OFF}) for each event.

events, weakening atmospheric stability. A relatively higher θ_e and weaker θ gradient in AH_{ON} during the prestorm period indicates that AH helps to prime the PBL for convective activity.

Analysis of pressure velocity in the prestorm period indicates that, even before the onset of precipitation, there is a tendency for stronger upward motion (stronger negative ω) in AH_{ON} relative to AH_{OFF}. During the onset of precipitation, this prestorm difference in ω rapidly increases, with AH_{ON} showing faster and stronger development of convective upward motion throughout the PBL (Fig. 10).

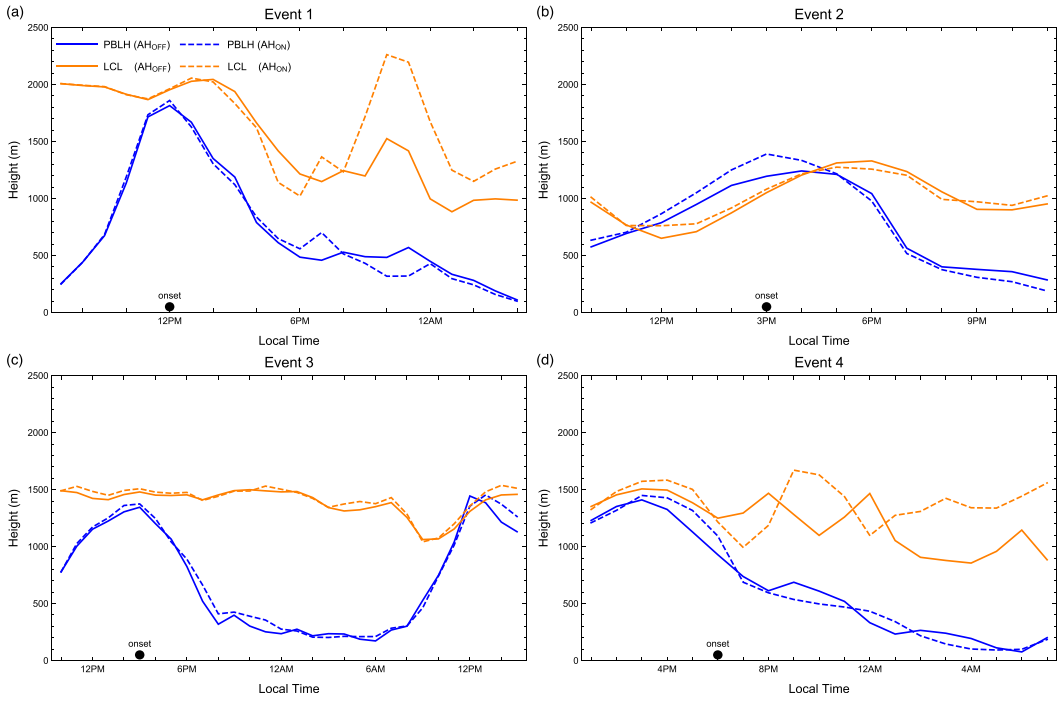

FIG. 9. Temporal profile of urban-averaged PBL height and LCL in AH_{ON} and AH_{OFF} for each event.

Enhanced updraft is associated with stronger convergence in AH_{ON} relative to AH_{OFF}. Figure 11 shows peak hour convergence at 750 hPa during the rainfall period. Enhanced convergence is found in AH_{ON}, especially in the high-density residential and commercial areas. The spatial distribution of convergence features varies by event, but for the heavy rainfall events (events 1 and 4) there is a tendency for the convergence zones to shift from the border to the center of the city in AH_{ON} relative to AH_{OFF}. This result is important because it shows that AH has the potential to influence the distribution of rainfall within and around the urban core, in addition to any impacts that urban surface representation has on the simulated propagation of storm cells (Bornstein and Lin 2000; Miao et al. 2009).

It should be noted that though high AH values are always found in commercial areas, which are in the central part of Beijing, the largest convergence zones are displaced from the city center in both AH_{ON} and AH_{OFF}. This might simply reflect the broader synoptic forcing of these rainfall events, which could favor storm

TABLE 3. Hourly averaged sensible heat, prestorm PBL height, MSE density within PBL height, vertical gradient of potential temperature (i.e., $\Delta\theta$), vertical gradient of equivalent potential temperature (i.e., $\Delta\theta_e$), and pressure velocity (i.e., ω) for averaged urban area and averaged commercial area in AH_{OFF} and its increase (in parentheses) in AH_{ON} relative to AH_{OFF} for each event.

	Sensible heat ($W\,m^{-2}$)	PBLH (m) (prestorm)	MSE density ($kJ\,kg^{-1}$)	$\Delta\theta$ (K) (prestorm)[a]	$\Delta\theta_e$ (K) (prestorm)[a]	ω ($Pa\,s^{-1}$) (prestorm)[b]
Urban area						
Event 1	131 (+6)	1006 (+20)	336.07 (+0.06)	0.7 (−0.1)	−3.6 (+0.3)	−0.22 (−0.02)
Event 2	127 (+26)	885 (+97)	336.57 (+0.32)	4.9 (−0.6)	−8.1 (+0.1)	−0.04 (−0.10)
Event 3	168 (+14)	1135 (+26)	349.13 (+0.01)	3.5 (−0.2)	−10.7 (+0.6)	−0.19 (−0.01)
Event 4	94 (+16)	1229 (+73)	352.32 (−1.00)	3.6 (−0.2)	−11.4 (+1.2)	−0.26 (−0.17)
Commercial area						
Event 1	187 (+26)	1061 (+73)	337.50 (+0.09)	0.5 (−0.2)	−3.3 (+0.9)	−0.59 (−0.07)
Event 2	161 (+76)	896 (+209)	335.92 (+0.73)	4.3 (−0.7)	−7.2 (+0.5)	0.01 (−0.41)
Event 3	230 (+54)	1220 (+54)	349.25 (+0.00)	2.9 (−0.4)	−10.0 (+1.2)	−0.13 (−0.20)
Event 4	145 (+49)	1422 (+86)	351.62 (−1.50)	2.8 (−1.0)	−10.2 (+3.5)	−0.33 (−0.70)

[a] Refers to (equivalent) potential temperature difference at 2000-m minus 500-m height.
[b] Values of ω refer to the pressure velocity at 1000 m.

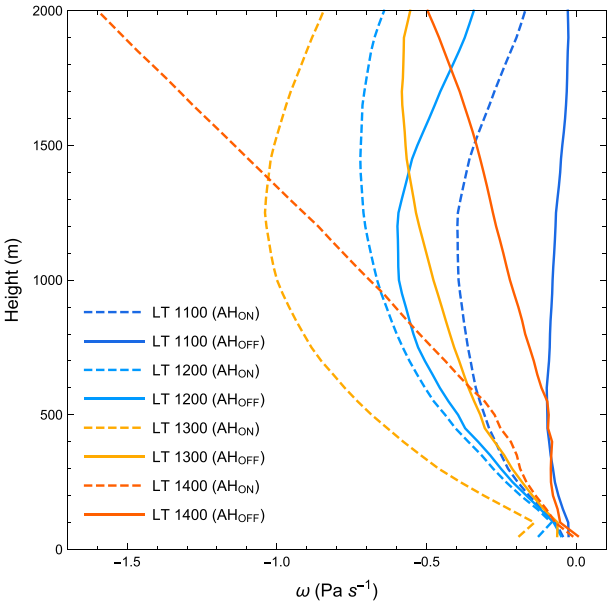

FIG. 10. Pressure velocity (i.e., ω) for 1100–1400 LT in the commercial area for event 1.

initiation at locations outside the urban core. It might also be influenced by the fact that the core commercial area has a relatively low percentage of pervious surface, leading to low latent heat flux and drier moisture condition compared to other land-cover types—that is, the energy partitioning effect noted in studies indicates that urbanization has a negative impact on precipitation (Zhang et al. 2009). In fact, the enhanced convergence zones are more likely to generate over the interface of three urban land covers and the urban–rural borders. Similar results were found in modeling studies of Houston (Shepherd et al. 2010) and Atlanta (Shem and Shepherd 2009). The studies of Houston and Atlanta, however, were not specific to AH—they considered the response to urban land cover—and concluded that the convergence pattern could be due to either dynamic (i.e., enhanced surface roughness) or thermodynamic (i.e., flux gradients) characteristics associated with urban land cover. However, in our study, as both the AH_{ON} and AH_{OFF} simulations include urban land-use characteristics, the tendency of convergence to cluster more clearly on land-cover boundaries in AH_{ON} appears to result from the thermodynamic condition alone (i.e., flux gradients associated with the spatial distribution of AH), which in turn appreciates the importance of separating the impacts of dynamic and thermodynamic conditions in studying the urban–atmosphere interactions (Zhu et al. 2016). More detailed analysis is needed in the future.

e. *Cumulative rainfall*

Results presented in sections 3b–d indicate that AH increases simulated sensible heat in the urban area, leading to enhanced turbulent energy flux and vertical air mixing over the city, a deeper PBL, and less stable conditions in the lower atmosphere. This is associated with small but systematically larger updraft during the prestorm period, rapid intensification of upward motion during the onset of precipitation, enhanced convergence during the maximum rainfall period, and larger atmospheric drydown during the storm, resulting in a higher poststorm LCL. Here we describe the net impact that these processes have on the magnitude and distribution of rainfall.

Maps of cumulative precipitation show that each event has a distinct spatial character: event 1 is concentrated on the southeastern edge of the city and events 2 and 3 have rain in the northern portion of the domain, while rain in event 4 is distributed across much of the domain (Figs. 12a–d). In all cases the 500-hPa background winds are generally oriented from the west, but they range from southwesterly (event 1) to northwesterly (event 2). Rainfall differences between AH_{ON} and AH_{OFF} are not as clearly structured as the differences in surface fields, but all four events show increased rainfall in the urban area and surroundings under AH_{ON} compared with AH_{OFF}. This general increase suggests that AH may have the potential to modulate rainfall by increasing the energy available for convection, and the localization of the rainfall enhancement is a result of small shifts in convection cells and background winds across the domain. This enhancement is also consistent with the results of Feng et al. (2012) for Beijing–Tianjin–Hebei region at larger spatiotemporal scale analysis.

It is interesting to note, however, that the timing of enhancement differs across events (Fig. 13). For events 1 and 3, cumulative rainfall is larger in AH_{ON} during the whole process, suggesting that rainfall of these events is triggered earlier because of AH; however, for events 2 and 4, the evolution of rainfall lags behind in AH_{ON} for a period of time and then exceeds the amount in AH_{OFF} later. This suggests that AH acts to increase precipitation yield even if the initial onset is delayed. The difference between these temporal patterns could reflect the fact that AH influences rainfall through multiple mechanisms. In some cases, AH causes the PBL to deepen to the LCL faster in AH_{ON} than AH_{OFF} when there can be an earlier onset of rainfall, while in other cases entrainment at the top of the PBL can actually delay the onset of rain, but destabilization of the lower atmosphere due to AH eventually leads to deeper convection and more total rainfall.

Previous research has shown that urbanization can influence rainfall patterns through multiple mechanisms

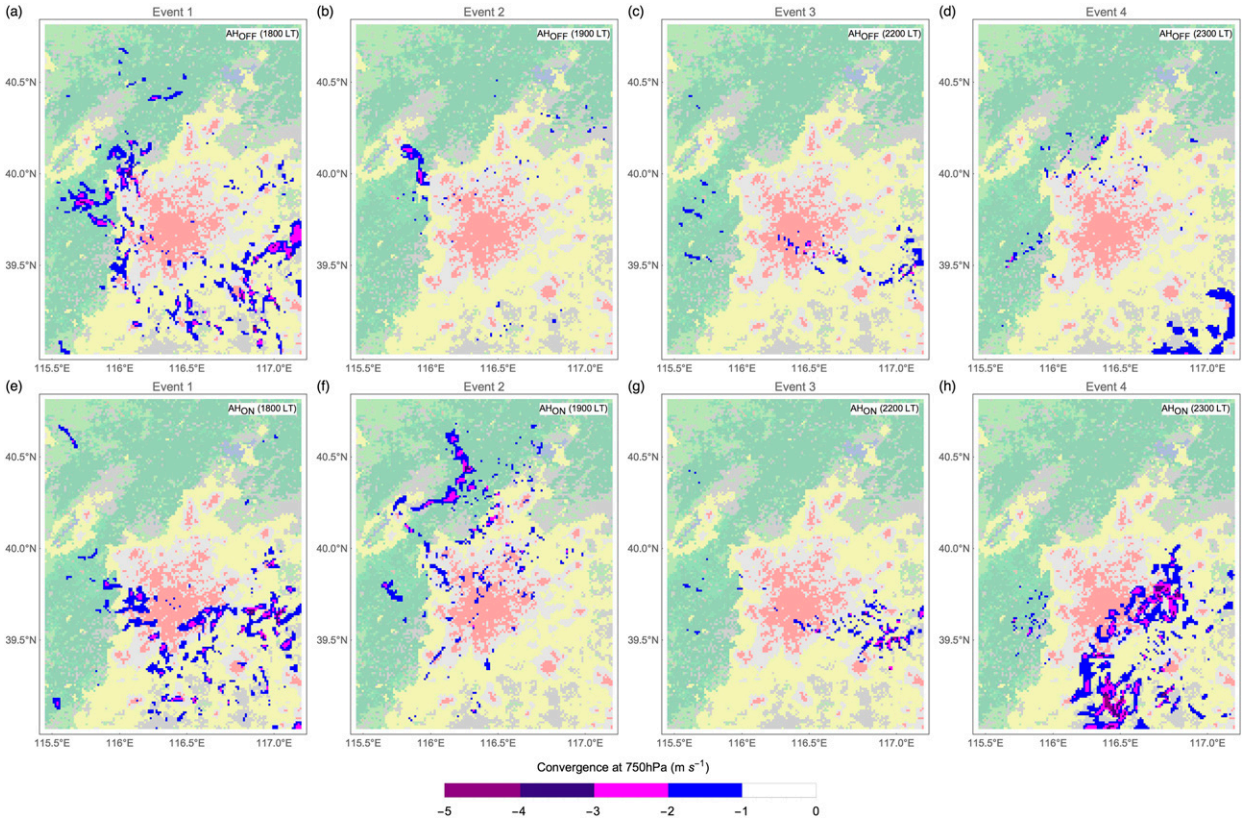

FIG. 11. Low-level convergence at 750 hPa during the convective period for each event in AH_{OFF} at (a) 1800, (b) 1900, (c) 2200, and (d) 2300 LT and in AH_{ON} at (e) 1800, (f) 1900, (g) 2200, and (h) 2300 LT. The underlying color rasters denote land uses (cf. Fig. 1).

that would be active at different points in the convection process, including impacts on low-level moisture and direct heating due to the UHI effect (Bornstein and Lin 2000; Dixon and Mote 2003; Shem and Shepherd 2009). Our study differs from this previous work in that we are specifically concerned with AH, rather than with the entire UHI phenomenon. Nevertheless, we see some mechanistic consistency in the fact that heating associated with the urban core can influence convection through impacts on stability and moisture. We do caution that our analysis only considers AH and intentionally excludes the multiple factors known to contribute to the UHI as a whole (e.g., surface thermal properties, urban geometry, vegetation effects, and pollution). The AH signal that we see in our simulations suggests a systematic effect on rainfall, but the magnitude of this signal is small relative to the full urban impact on precipitation process.

4. Conclusions

This study investigated the impact of anthropogenic heat on summertime urban rainfall events in Beijing. To explore the mechanism of this impact, we conducted controlled simulations (AH_{OFF}) and identical simulations with AH (AH_{ON}) for four summer rainfall events using BEP-BEM within the WRF Model. The main findings are as follows and are summarized in Fig. 14:

1) Anthropogenic heat (AH) exerts a large impact on surface energy balance, primarily by increasing sensible heat flux. Considering the high heat admittance of the building materials, AH is largest for commercial areas, which are more densely built up than the other two urban categories, and has the greatest impact on sensible heat flux in these areas.
2) Increase in sensible heat due to AH leads to a higher PBL height during the prestorm period in AH_{ON} for all events, though the magnitude of the difference varies between events. This deeper PBL has approximately the same MSE density as in AH_{OFF}, indicating that AH_{ON} has deeper penetration of relatively high energy, turbulent PBL air, which can increase the potential for triggering convection.
3) Reduced stability within the PBL is observed during the prestorm period, as evident in the vertical gradient of potential temperature, equivalent potential

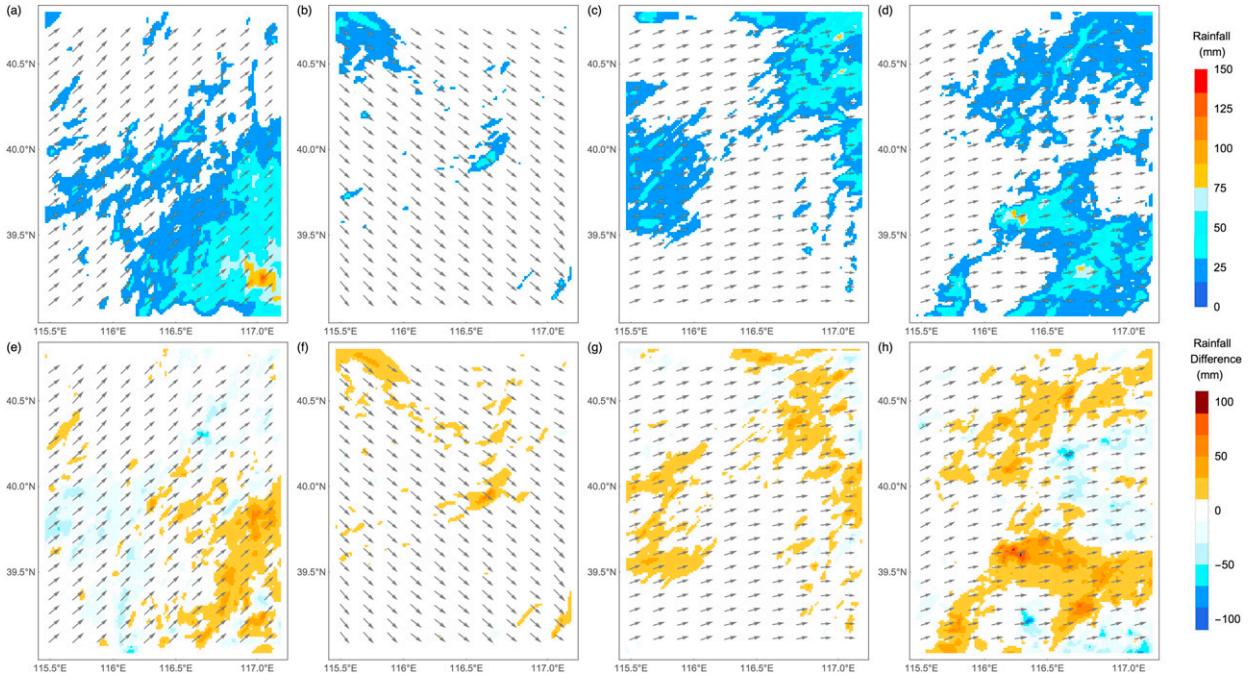

FIG. 12. Spatial distribution of cumulative rainfall and horizontal background wind speed at 500 hPa for (a) event 1, (b) event 2, (c) event 3, and (d) event 4 in AH_{ON} and its difference compared to AH_{OFF} for (e) event 1, (f) event 2, (g) event 3, and (h) event 4.

temperature, and pressure velocity. This destabilization and updraft provides conditions that are more favorable to the development of convective precipitation.

4) During the storm event, convergence is more intense and tends to penetrate into the urban area in AH_{ON} relative to AH_{OFF}. In particular, the strongest convergence zones form on the border rather than core areas of LIR/HIR or HIR/CIT where high AH emissions occur. The fact that this urban boundary effect is observed in our AH_{ON} versus AH_{OFF} simulations suggests that the phenomena can be triggered by heating contrasts alone. Shem and Shepherd (2009) identified this border effect due to urban land cover and hypothesized that it was due to roughness effects and/or flux gradients. Since roughness is identical in the AH_{ON} and AH_{OFF} simulations, only heating contrasts can explain the result in our simulations.
5) Although the AH influence on cumulative rainfall in these simulations is an increase in all events, this result should be interpreted with caution, as the AH influence is small relative to model uncertainty for some events. The temporal evolution of rainfall in AH_{ON} relative to AH_{OFF}, however, differs between events according to the synoptic conditions, suggesting that multiple mechanisms are involved in enhancing precipitation. AH can trigger earlier initialization of rainfall for conditions of locally driven convection, through PBL growth and local destabilization of the lower atmosphere, and it may also enhance total precipitation yield during a rainfall event because of greater available energy for convection.

The possible pathways of AH in influence on urban summertime rainfall identified in this study are summarized in Fig. 14: anthropogenic heat emission increases sensible heat flux, enhances mixing and turbulent energy transport, lifts PBL height, increases dry static energy, and destabilizes the atmosphere in urban areas through thermal perturbation and strong updraft during the prestorm period. This results in enhanced convergence during the major rainfall period. Intensified rainfall leads to greater atmospheric drydown during the storm and a higher poststorm LCL. Therefore, AH may enhance urban rainfall and may also modify the spatial pattern of the rainfall.

This study advances a small but growing literature on the impact that AH has on urban hydrometeorology by comparing AH_{ON} and AH_{OFF} simulations that both include urban morphology. Considering the substantial magnitude of AH emission compared with other urban energy balance terms and its potential impact on urban turbulence transport, PBL development, and atmospheric instability, we suggest that anthropogenic heat should be considered when performing NWP or model-based

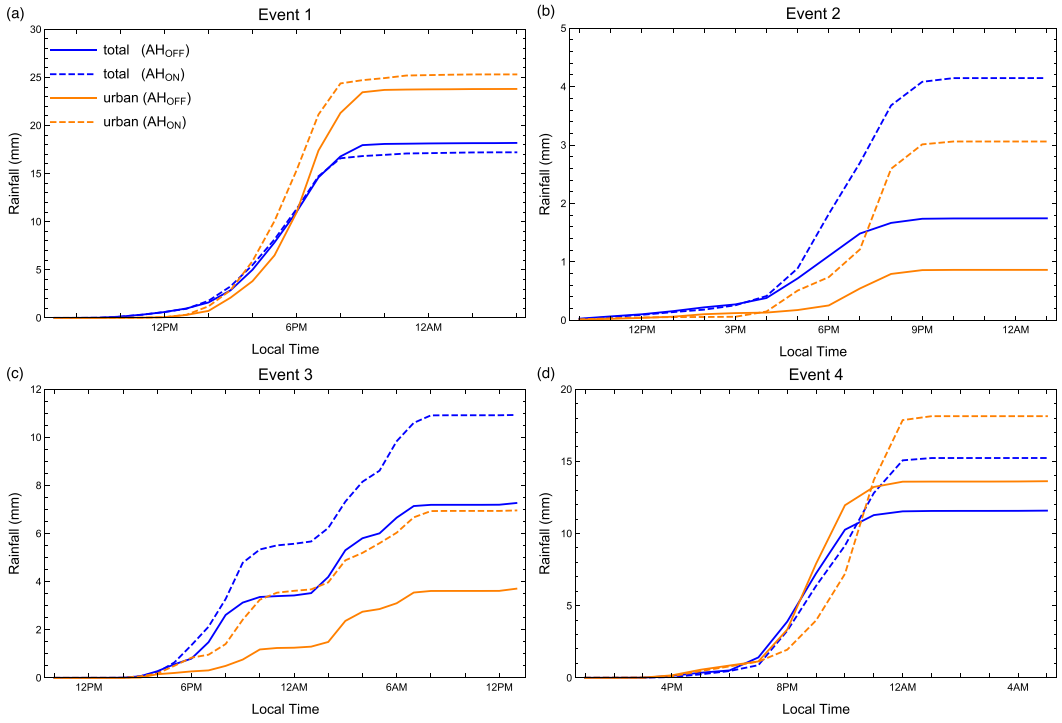

FIG. 13. Urban- and D03-averaged cumulative rainfall in AH_{ON} and AH_{OFF} for each event.

regional climate studies in urban areas. The use of BEP-BEM provides a widely applicable and easily accessible way to obtain dynamic spatiotemporal AH estimates for nonindustrial cities where buildings contribute the dominant part of total anthropogenic heat.

This study does have certain limitations that are important to appreciate. First, the conclusions are drawn from four short rainfall events in Beijing. More events of different rainfall types in multiple locations need to be examined to overcome the limitation of a short record in a single city. In addition, although the AH impact on PBL and atmospheric instability is consistent for all simulated events, its impact on rainfall may be influenced by external factors (e.g., background synoptic condition and moisture availability) that require further exploration. Also, to fully verify the proposed mechanism by which AH influences urban rainfall, future work is required to extend this study to include other sources of AH beyond the building sector. Evaluation of these high-resolution rainfall simulations is also a challenge for the community. The urban rainfall monitoring network used in this study was only recently deployed, and its coverage could still be improved (Yang et al. 2015). As the data record grows, it will be possible to study model performance for a larger number of summer rainfall events and to achieve more robust assessment of the influence of AH on model performance.

Acknowledgments. This work was supported by funding from the National Natural Science Foundation of China (NSFC) under Grants 51190092 and 51409147, the Ministry of Science and Technology of China under

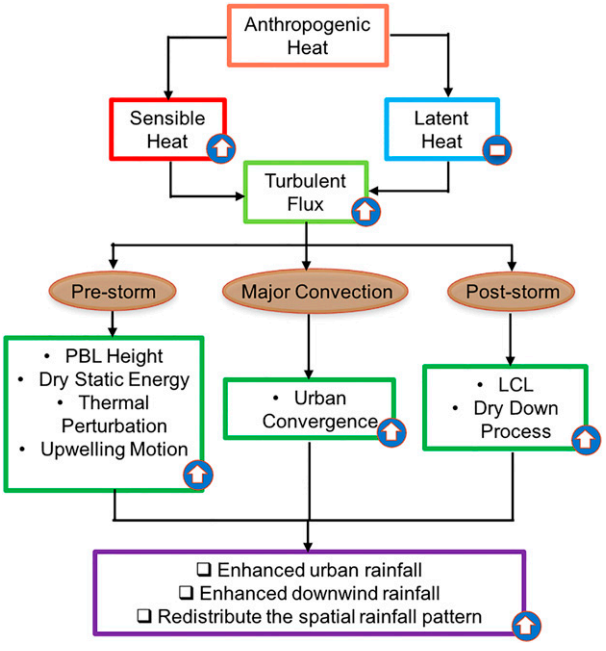

FIG. 14. A proposed framework for the mechanism of AH impact on urban rainfall.

Grant 2013DFG72270, and China Postdoctoral Science Foundation under Grant 2015T80093. The simulations were performed on the supercomputing clusters of Tsinghua National Laboratory for Information Science and Technology. We thank Dr. Shiguang Miao and Dr. Junxia Dou from the Institute of Urban Meteorology, China Meteorological Administration, and Dr. Aizhong Hou from the Ministry of Water Resources, China, for providing the observational data. We thank Editor Dr. Faisal Hossain and three reviewers for their insightful and constructive comments that significantly improved the quality of this work.

REFERENCES

Andreae, M. O., D. Rosenfeld, P. Artaxo, A. Costa, G. Frank, K. Longo, and M. Silva-Dias, 2004: Smoking rain clouds over the Amazon. *Science*, **303**, 1337–1342, doi:10.1126/science.1092779.

Arnfield, A. J., 2003: Two decades of urban climate research: A review of turbulence, exchanges of energy and water, and the urban heat island. *Int. J. Climatol.*, **23**, 1–26, doi:10.1002/joc.859.

——, and C. Grimmond, 1998: An urban canyon energy budget model and its application to urban storage heat flux modeling. *Energy Build.*, **27**, 61–68, doi:10.1016/S0378-7788(97)00026-1.

Ashley, W. S., M. L. Bentley, and J. A. Stallins, 2012: Urban-induced thunderstorm modification in the southeast United States. *Climatic Change*, **113**, 481–498, doi:10.1007/s10584-011-0324-1.

Baugh, K., C. D. Elvidge, T. Ghosh, and D. Ziskin, 2010: Development of a 2009 stable lights product using DMSP-OLS data. *Proc. Asia-Pac. Adv. Network*, **30**, 114–130, doi:10.7125/APAN.30.17.

Benson-Lira, V., M. Georgescu, S. Kaplan, and E. Vivoni, 2016: Loss of a lake system in a megacity: The impact of urban expansion on seasonal meteorology in Mexico City. *J. Geophys. Res. Atmos.*, **121**, 3079–3099, doi:10.1002/2015JD024102.

Best, M., and C. Grimmond, 2016: Investigation of the impact of anthropogenic heat flux within an urban land surface model and PILPS-urban. *Theor. Appl. Climatol.*, **126**, 51–60, doi:10.1007/s00704-015-1554-3.

Bohnenstengel, S., I. Hamilton, M. Davies, and S. Belcher, 2014: Impact of anthropogenic heat emissions on London's temperatures. *Quart. J. Roy. Meteor. Soc.*, **140**, 687–698, doi:10.1002/qj.2144.

Bornstein, R., and M. LeRoy, 1990: Urban barrier effects on convective and frontal thunderstorms. Preprints, *Fourth Conf. on Mesoscale Processes*, Boulder, CO, Amer. Meteor. Soc., 25–29.

——, and Q. Lin, 2000: Urban heat islands and summertime convective thunderstorms in Atlanta: Three case studies. *Atmos. Environ.*, **34**, 507–516, doi:10.1016/S1352-2310(99)00374-X.

Cadet, D., 1983: Metromex: A review and summary. *Eos, Trans. Amer. Geophys. Union*, **64**, 50–51, doi:10.1029/EO064i006p00050-02.

Changnon, S. A., and N. E. Westcott, 2002: Heavy rainstorms in Chicago: Increasing frequency, altered impacts, and future implications. *J. Amer. Water Resour. Assoc.*, **38**, 1467–1475, doi:10.1111/j.1752-1688.2002.tb04359.x.

Chen, F., X. Yang, and W. Zhu, 2014: WRF simulations of urban heat island under hot-weather synoptic conditions: The case study of Hangzhou City, China. *Atmos. Res.*, **138**, 364–377, doi:10.1016/j.atmosres.2013.12.005.

——, ——, and J. Wu, 2016: Simulation of the urban climate in a Chinese megacity with spatially heterogeneous anthropogenic heat data. *J. Geophys. Res. Atmos.*, **121**, 5193–5212, doi:10.1002/2015JD024642.

Diem, J. E., and D. P. Brown, 2003: Anthropogenic impacts on summer precipitation in central Arizona, USA. *Prof. Geogr.*, **55**, 343–355.

Dixon, P. G., and T. L. Mote, 2003: Patterns and causes of Atlanta's urban heat island–initiated precipitation. *J. Appl. Meteor.*, **42**, 1273–1284, doi:10.1175/1520-0450(2003)042<1273:PACOAU>2.0.CO;2.

Elvidge, C. D., K. E. Baugh, E. A. Kihn, H. W. Kroehl, and E. R. Davis, 1997: Mapping city lights with nighttime data from the DMSP Operational Linescan System. *Photogramm. Eng. Remote Sensing*, **63**, 727–734.

Evans, J. P., M. Ekström, and F. Ji, 2012: Evaluating the performance of a WRF physics ensemble over south-east Australia. *Climate Dyn.*, **39**, 1241–1258, doi:10.1007/s00382-011-1244-5.

Fan, H., and D. J. Sailor, 2005: Modeling the impacts of anthropogenic heating on the urban climate of Philadelphia: A comparison of implementations in two PBL schemes. *Atmos. Environ.*, **39**, 73–84, doi:10.1016/j.atmosenv.2004.09.031.

Feng, J.-M., Y.-L. Wang, Z.-G. Ma, and Y.-H. Liu, 2012: Simulating the regional impacts of urbanization and anthropogenic heat release on climate across China. *J. Climate*, **25**, 7187–7203, doi:10.1175/JCLI-D-11-00333.1.

Flanner, M. G., 2009: Integrating anthropogenic heat flux with global climate models. *Geophys. Res. Lett.*, **36**, L02801, doi:10.1029/2008GL036465.

Grimmond, C., and T. R. Oke, 2002: Turbulent heat fluxes in urban areas: Observations and a Local-Scale Urban Meteorological Parameterization Scheme (LUMPS). *J. Appl. Meteor.*, **41**, 792–810, doi:10.1175/1520-0450(2002)041<0792:THFIUA>2.0.CO;2.

——, J. Salmond, T. R. Oke, B. Offerle, and A. Lemonsu, 2004: Flux and turbulence measurements at a densely built-up site in Marseille: Heat, mass (water and carbon dioxide), and momentum. *J. Geophys. Res.*, **109**, D24101, doi:10.1029/2004JD004936.

——, and Coauthors, 2010: The international urban energy balance models comparison project: First results from phase 1. *J. Appl. Meteor. Climatol.*, **49**, 1268–1292, doi:10.1175/2010JAMC2354.1.

Guo, X., D. Fu, and J. Wang, 2006: Mesoscale convective precipitation system modified by urbanization in Beijing city. *Atmos. Res.*, **82**, 112–126, doi:10.1016/j.atmosres.2005.12.007.

Gutiérrez, E., J. E. González, R. Bornstein, M. Arend, and A. Martilli, 2013: A new modeling approach to forecast building energy demands during extreme heat events in complex cities. *J. Sol. Energy Eng.*, **135**, 040906, doi:10.1115/1.4025510.

Haberlie, A. M., W. S. Ashley, and T. J. Pingel, 2015: The effect of urbanisation on the climatology of thunderstorm initiation. *Quart. J. Roy. Meteor. Soc.*, **141**, 663–675, doi:10.1002/qj.2499.

Hamilton, I. G., M. Davies, P. Steadman, A. Stone, I. Ridley, and S. Evans, 2009: The significance of the anthropogenic heat emissions of London's buildings: A comparison against captured shortwave solar radiation. *Build. Environ.*, **44**, 807–817, doi:10.1016/j.buildenv.2008.05.024.

Hand, L. M., and J. M. Shepherd, 2009: An investigation of warm-season spatial rainfall variability in Oklahoma City: Possible linkages to urbanization and prevailing wind. *J. Appl. Meteor. Climatol.*, **48**, 251–269, doi:10.1175/2008JAMC2036.1.

Hong, S.-Y., J. Dudhia, and S.-H. Chen, 2004: A revised approach to ice microphysical processes for the bulk parameterization of clouds and precipitation. *Mon. Wea. Rev.*, **132**, 103–120, doi:10.1175/1520-0493(2004)132<0103:ARATIM>2.0.CO;2.

Huang, Q., X. Yang, B. Gao, Y. Yang, and Y. Zhao, 2014: Application of DMSP/OLS nighttime light images: A meta-analysis and a systematic literature review. *Remote Sens.*, **6**, 6844–6866, doi:10.3390/rs6086844.

Ichinose, T., K. Shimodozono, and K. Hanaki, 1999: Impact of anthropogenic heat on urban climate in Tokyo. *Atmos. Environ.*, **33**, 3897–3909, doi:10.1016/S1352-2310(99)00132-6.

Janjić, Z. I., 1994: The step-mountain eta coordinate model: Further developments of the convection, viscous sublayer, and turbulence closure schemes. *Mon. Wea. Rev.*, **122**, 927–945, doi:10.1175/1520-0493(1994)122<0927:TSMECM>2.0.CO;2.

Jankov, I., W. A. Gallus Jr., M. Segal, B. Shaw, and S. E. Koch, 2005: The impact of different WRF Model physical parameterizations and their interactions on warm season MCS rainfall. *Wea. Forecasting*, **20**, 1048–1060, doi:10.1175/WAF888.1.

Johnson, D. B., 1982: The role of giant and ultragiant aerosol particles in warm rain initiation. *J. Atmos. Sci.*, **39**, 448–460, doi:10.1175/1520-0469(1982)039<0448:TROGAU>2.0.CO;2.

Kishtawal, C. M., D. Niyogi, M. Tewari, R. A. Pielke, and J. M. Shepherd, 2010: Urbanization signature in the observed heavy rainfall climatology over India. *Int. J. Climatol.*, **30**, 1908–1916, doi:10.1002/joc.2044.

Lei, M., D. Niyogi, C. Kishtawal, R. Pielke Sr., A. Beltrán-Przekurat, T. Nobis, and S. Vaidya, 2008: Effect of explicit urban land surface representation on the simulation of the 26 July 2005 heavy rain event over Mumbai, India. *Atmos. Chem. Phys.*, **8**, 5975–5995, doi:10.5194/acp-8-5975-2008.

Lu, D., H. Tian, G. Zhou, and H. Ge, 2008: Regional mapping of human settlements in southeastern China with multisensor remotely sensed data. *Remote Sens. Environ.*, **112**, 3668–3679, doi:10.1016/j.rse.2008.05.009.

Mahmood, R., and Coauthors, 2014: Land cover changes and their biogeophysical effects on climate. *Int. J. Climatol.*, **34**, 929–953, doi:10.1002/joc.3736.

Masson, V., C. Grimmond, and T. R. Oke, 2002: Evaluation of the Town Energy Balance (TEB) scheme with direct measurements from dry districts in two cities. *J. Appl. Meteor.*, **41**, 1011–1026, doi:10.1175/1520-0450(2002)041<1011:EOTTEB>2.0.CO;2.

Miao, S., F. Chen, M. A. LeMone, M. Tewari, Q. Li, and Y. Wang, 2009: An observational and modeling study of characteristics of urban heat island and boundary layer structures in Beijing. *J. Appl. Meteor. Climatol.*, **48**, 484–501, doi:10.1175/2008JAMC1909.1.

Narumi, D., A. Kondo, and Y. Shimoda, 2009: Effects of anthropogenic heat release upon the urban climate in a Japanese megacity. *Environ. Res.*, **109**, 421–431, doi:10.1016/j.envres.2009.02.013.

Nie, W.-S., 2015: Spatialtemporal characteristics of anthropogenic heat in an urban environment and impacts on hydrometeorology. MSc thesis, Department of Hydraulic Engineering, Tsinghua University, 98 pp.

——, T. Sun, and G.-H. Ni, 2014: Spatiotemporal characteristics of anthropogenic heat in an urban environment: A case study of Tsinghua campus. *Build. Environ.*, **82**, 675–686, doi:10.1016/j.buildenv.2014.10.011.

Niyogi, D., T. Holt, S. Zhong, P. C. Pyle, and J. Basara, 2006: Urban and land surface effects on the 30 July 2003 mesoscale convective system event observed in the southern Great Plains. *J. Geophys. Res.*, **111**, D19107, doi:10.1029/2005JD006746.

——, P. Pyle, M. Lei, S. Arya, C. Kishtawal, M. Shepherd, F. Chen, and B. Wolfe, 2011: Urban modification of thunderstorms: An observational storm climatology and model case study for the Indianapolis urban region. *J. Appl. Meteor. Climatol.*, **50**, 1129–1144, doi:10.1175/2010JAMC1836.1.

Nobis, T. E., 2007: Coupling an urban parameterization to an atmospheric model using an operational configuration. Ph.D. thesis, Colorado State University, 182 pp. [Available online at http://hdl.handle.net/10217/40473.]

Pielke, R. A., Sr., and Y. Mahrer, 1978: Verification analysis of the University of Virginia three-dimensional mesoscale model prediction over south Florida for 1 July 1973. *Mon. Wea. Rev.*, **106**, 1568–1589, doi:10.1175/1520-0493(1978)106<1568:VAOTUO>2.0.CO;2.

——, J. Adegoke, A. Beltrán-Przekurat, C. Hiemstra, J. Lin, U. Nair, D. Niyogi, and T. Nobis 2007: An overview of regional land-use and land-cover impacts on rainfall. *Tellus*, **59B**, 587–601, doi:10.1111/j.1600-0889.2007.00251.x.

——, and Coauthors, 2011: Land use/land cover changes and climate: Modeling analysis and observational evidence. *Wiley Interdiscip. Rev.: Climate Change*, **2**, 828–850, doi:10.1002/wcc.144.

Ramanathan, V., P. Crutzen, J. Kiehl, and D. Rosenfeld, 2001: Aerosols, climate, and the hydrological cycle. *Science*, **294**, 2119–2124, doi:10.1126/science.1064034.

Rosenfeld, D., 2000: Suppression of rain and snow by urban and industrial air pollution. *Science*, **287**, 1793–1796, doi:10.1126/science.287.5459.1793.

——, U. Lohmann, G. B. Raga, C. D. O'Dowd, M. Kulmala, S. Fuzzi, A. Reissell, and M. O. Andreae, 2008: Flood or drought: How do aerosols affect precipitation? *Science*, **321**, 1309–1313, doi:10.1126/science.1160606.

Ryu, Y.-H., J.-J. Baik, and S.-H. Lee, 2013: Effects of anthropogenic heat on ozone air quality in a megacity. *Atmos. Environ.*, **80**, 20–30, doi:10.1016/j.atmosenv.2013.07.053.

Sailor, D. J., 2009: Quantifying anthropogenic moisture emissions and their potential impact on the urban climate. *Eighth Symp. on the Urban Environment*, Phoenix, AZ, Amer. Meteor. Soc., 2.2. [Available online at https://ams.confex.com/ams/89annual/techprogram/paper_150461.htm.]

——, 2011: A review of methods for estimating anthropogenic heat and moisture emissions in the urban environment. *Int. J. Climatol.*, **31**, 189–199, doi:10.1002/joc.2106.

——, M. Georgescu, J. M. Milne, and M. A. Hart, 2015: Development of a national anthropogenic heating database with an extrapolation for international cities. *Atmos. Environ.*, **118**, 7–18, doi:10.1016/j.atmosenv.2015.07.016.

Salamanca, F., A. Krpo, A. Martilli, and A. Clappier, 2010: A new building energy model coupled with an urban canopy parameterization for urban climate simulations—Part I. Formulation, verification, and sensitivity analysis of the model. *Theor. Appl. Climatol.*, **99**, 331–344, doi:10.1007/s00704-009-0142-9.

——, M. Georgescu, A. Mahalov, M. Moustaoui, M. Wang, and B. Svoma, 2013: Assessing summertime urban air conditioning consumption in a semiarid environment. *Environ. Res. Lett.*, **8**, 034022, doi:10.1088/1748-9326/8/3/034022.

Santamouris, M., 2013: *Energy and Climate in the Urban Built Environment.* Routledge, 410 pp.

Shem, W., and M. Shepherd, 2009: On the impact of urbanization on summertime thunderstorms in Atlanta: Two numerical model case studies. *Atmos. Res.*, **92**, 172–189, doi:10.1016/j.atmosres.2008.09.013.

Shepherd, J. M., 2005: A review of current investigations of urban-induced rainfall and recommendations for the future. *Earth Interact.*, **9**, doi:10.1175/EI156.1.

——, and S. J. Burian, 2003: Detection of urban-induced rainfall anomalies in a major coastal city. *Earth Interact.*, **7**, doi:10.1175/1087-3562(2003)007<0001:DOUIRA>2.0.CO;2.

——, H. Pierce, and A. J. Negri, 2002: Rainfall modification by major urban areas: Observations from spaceborne rain radar on the TRMM satellite. *J. Appl. Meteor.*, **41**, 689–701, doi:10.1175/1520-0450(2002)041<0689:RMBMUA>2.0.CO;2.

——, M. Carter, M. Manyin, D. Messen, and S. Burian, 2010: The impact of urbanization on current and future coastal precipitation: A case study for Houston. *Environ. Plann. B*, **37**, 284–304, doi:10.1068/b34102t.

Simmonds, I., and K. Keay, 1997: Weekly cycle of meteorological variations in Melbourne and the role of pollution and anthropogenic heat release. *Atmos. Environ.*, **31**, 1589–1603, doi:10.1016/S1352-2310(96)00344-5.

Skamarock, W. C., J. B. Klemp, J. Dudhia, D. O. Gill, D. M. Barker, W. Wang, and J. G. Powers, 2005: A description of the Advanced Research WRF version 2. NCAR Tech. Note NCAR/TN-468+STR, 88 pp., doi:10.5065/D6DZ069T.

Sun, T., C. Grimmond, and G. H. Ni, 2016: How do green roofs mitigate urban thermal stress under heat waves? *J. Geophys. Res. Atmos.*, **121**, 5320–5335, doi:10.1002/2016JD024873.

Taha, H., 1997: Urban climates and heat islands: Albedo, evapotranspiration, and anthropogenic heat. *Energy Build.*, **25**, 99–103, doi:10.1016/S0378-7788(96)00999-1.

Thielen, J., W. Wobrock, A. Gadian, P. Mestayer, and J.-D. Creutin, 2000: The possible influence of urban surfaces on rainfall development: A sensitivity study in 2D in the meso-γ-scale. *Atmos. Res.*, **54**, 15–39, doi:10.1016/S0169-8095(00)00041-7.

Wilby, R. L., and G. L. Perry, 2006: Climate change, biodiversity and the urban environment: A critical review based on London, UK. *Prog. Phys. Geogr.*, **30**, 73–98, doi:10.1191/0309133306pp470ra.

Yang, L., F. Tian, J. A. Smith, and H. Hu, 2014: Urban signatures in the spatial clustering of summer heavy rainfall events over the Beijing metropolitan region. *J. Geophys. Res. Atmos.*, **119**, 1203–1217, doi:10.1002/2013JD020762.

Yang, W.-Y., Z. Li, T. Sun, and G.-H. Ni, 2016: Better knowledge with more gauges? Investigation of the spatiotemporal characteristics of precipitation variations over the greater Beijing region. *Int. J. Climatol.*, **36**, 3607–3619, doi:10.1002/joc.4579.

Yu, M., and Y. Liu, 2015: The possible impact of urbanization on a heavy rainfall event in Beijing. *J. Geophys. Res. Atmos.*, **120**, 8132–8143, doi:10.1002/2015JD023336.

——, G. R. Carmichael, T. Zhu, and Y. Cheng, 2014: Sensitivity of predicted pollutant levels to anthropogenic heat emissions in Beijing. *Atmos. Environ.*, **89**, 169–178, doi:10.1016/j.atmosenv.2014.01.034.

Zhang, C. L., F. Chen, S. G. Miao, Q. C. Li, X. A. Xia, and C. Y. Xuan, 2009: Impacts of urban expansion and future green planting on summer precipitation in the Beijing metropolitan area. *J. Geophys. Res.*, **114**, D02116, doi:10.1029/2008JD010328.

Zhu, X., G. Ni, Z. Cong, T. Sun, and D. Li, 2016: Impacts of surface heterogeneity on dry planetary boundary layers in an urban–rural setting. *J. Geophys. Res. Atmos.*, **121**, 12 164–12 179, doi:10.1002/2016JD024982.